Photon-number-resolving detector with 10 bits of resolution

Leaf A. Jiang,* Eric A. Dauler, and Joshua T. Chang
[1]*MIT Lincoln Laboratory, 244 Wood Street, Lexington, Massachusetts 02420, USA*
(Received 9 March 2007; published 21 June 2007)

A photon-number-resolving detector with single-photon resolution is described and demonstrated. It has 10 bits of resolution, does not require cryogenic cooling, and is sensitive to near ir wavelengths. This performance is achieved by flood illuminating a 32×32 element $In_xGa_{1-x}AsP$ Geiger-mode avalanche photodiode array that has an integrated counter and digital readout circuit behind each pixel.

DOI: 10.1103/PhysRevA.75.062325 PACS number(s): 03.67.Hk, 85.60.Gz, 42.50.Ar, 03.67.Lx

I. INTRODUCTION

Detectors that can resolve photon number have been shown to be useful for three-dimensional (3D) laser radar [1], coherent laser radar [2], linear optics quantum computing [3], characterization of single-photon sources [4], and quantum communications. Photon-number-resolving detectors to date have required cryogenic cooling [5], used time-multiplexing schemes that increase the net reset time [6], or involve a pulse-height discrimination process that suffers from multiplication noise [7]. Near ir or visible photon-number-resolving detectors with only 2–3 bits [5–7] of resolution have been reported thus far, where the number of bits is limited by multiplication noise [5,7] or measurement time [6]. Here we present a photon-number-resolving detector with 10 bits of resolution. This performance is achieved by a practical implementation of a $2^{10}=1024$ element detector cascade. The demonstrated detector cascade is ideally suited to applications that are loss-tolerant and require a relatively large dynamic range with sensitivities down to the single photon level, such as 3D laser radar and coherent laser radar. However, this type of detector array can also be applied to applications that are more sensitive to loss or dark counts by increasing the detection efficiency and optimizing the number of detector elements in the cascade.

The photon-number-resolving detector concept is illustrated in Fig. 1. Light from a laser or fiber is evenly illuminated on an array of nonmultiphoton-discriminating, single-photon detectors so that each pixel in the array has an equal chance of firing. If the array is large enough, then it is likely that multiple photons hit different pixels and the array can detect many photons simultaneously with a roughly constant detection efficiency over the whole array. Detector cascades with multiple bulk detector elements have been proposed [8] and compact integration of two photon-counting detector pixels has been demonstrated previously [9], but the present work demonstrates a compact, scalable, and practical implementation of a cascade of 1024 single-photon-counting detection elements.

The array of nonphoton-number-resolving, single photon detectors used in these experiments is a 32×32 array of $In_xGa_{1-x}AsP/InP$ Geiger-mode avalanche photodiodes (APDs) whose alloy composition is chosen for detection of 1.06 μm light. MIT Lincoln Laboratory has deployed many versions of these arrays in a number of laser radar systems [3]. The APD array is sealed into a hermetic package with a GaP microlens array (to improved the fill factor), thermoelectric cooler temperature control, and an integrated complementary metal-oxide semiconductor readout integrated circuit. The APDs used for the experiments in this paper are 30 μm in diameter on 100 μm pitch and are operated at −27 °C. Behind every pixel is a 2 GHz counter that records the time a given pixel fires. The time stamps for all pixels are read out and reset at a maximum rate of about 25 kHz through a custom electronics interface board and stored to RAID disk storage in real-time. There is currently a development effort at MIT Lincoln Laboratory to allow for continuous readout of the APDs, limited only by the APD reset time of about 1.6 μs for InP material [10].

II. EXPERIMENTAL SETUP

The experimental setup for characterizing our photon-number-resolving detector is shown in Fig. 2. The laser source is a fiber-coupled PicoQuant LDH-P-1064 nm subnanosecond pulse source at 1064 nm wavelength and operated at 20 kHz repetition rate. One channel of a Stanford Research Systems DG535 pulse generator is used to trigger the Geiger-mode APD array and a second channel is used to trigger the pulsed laser source. The timing jitter between the emission of the pulse and the trigger to the APD is measured to be less than 50 ps, limited by the channel-to-channel timing jitter of the oscilloscope that was used. The output of the pulsed laser is attenuated using an independently calibrated JDSU model HA9 fiber-coupled attenuator. The attenuation was set to 0 dB for laser power measurements or varied between 35 and 70 dB for quantum efficiency measurements. The light is delivered to the GM-APD array with an OzOptics LPC-02-1064-6/125-P-2.4-11AS-50-3A-3-2 fiber-pigtailed collimator. The laser beam's $1/e^2$ width was measured to be 2.1 mm with a Thorlabs WM100B beam width meter. The average output of the laser after the collimator with the attenuator set to 0 dB attenuation was measured to be −44.65 dBm. The pulse energy with 0 dB attenuation is computed at 1.7 pJ or 9.2×10^6 photons per pulse. The laser power did not drift more than ±0.5 dB during the measurements. Figure 3 shows the experimentally measured spatial profile of the probability of detection for the pulsed source at an average power of −94.65 dBm or 92 photons per pulse.

*Electronic address: leaf@ll.mit.edu

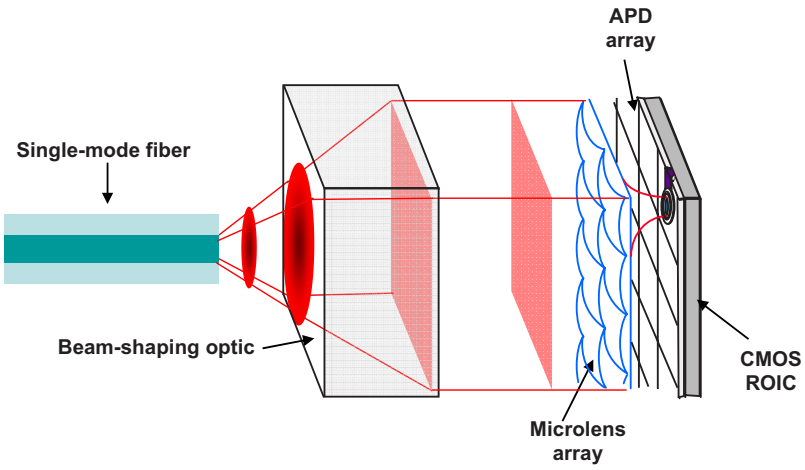

FIG. 1. (Color online) Photon-number-resolving detection concept using a large format array of single-photon detectors.

The vertical and horizontal cross-sections of beam profile in Fig. 3 have a shape that is slightly more complicated than a simple Gaussian. The peaks and tails of the cross sections fit well to a Gaussian function with a $1/e^2$ width of 1.6 and 2.0 mm, respectively. This measurement agrees fairly well with the Thorlabs beam width meter. There are 45 bad pixels—pixels that never register a photon hit—in this particular APD array, most of which are along the edges of the array and hence do not significantly influence the detector efficiency measurements. The pulse was timed to hit the array after the arrival of the APD trigger. In the experiments presented here, the APDs were active for 122 ns before the optical pulse arrived.

The dark counts for this particular array were measured at 160 k counts/s per pixel when operated at −27 °C, although other InP detector arrays at MIT Lincoln Laboratory have demonstrated dark counts as low as 65 000 counts/s per pixel at room temperature [10] and 10 000 counts/s per pixel with thermoelectric cooling. The aggregate dark count rate increases with detector area and so there is a limit to the largest useful array size for a given operating temperature. Our detector array has a rather large total active area of 0.50 mm^2 but reducing the individual APD active areas can result in roughly an order of magnitude reduction of dark counts without sacrificing photon-detection efficiency [11] or photon-number resolution. In addition, further improvements in dark counts should be possible with better material quality and the removal of shallow electron traps.

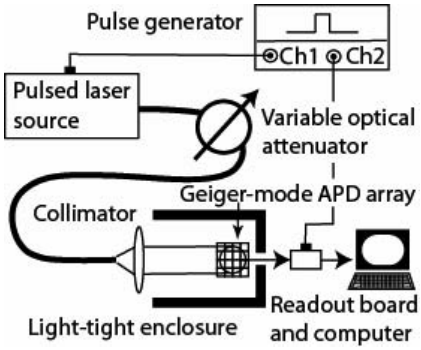

FIG. 2. Experimental setup for the test of the photon-number-resolving detector.

III. PHOTON-DETECTION EFFICIENCY

The photon-detection efficiency (PDE) is defined as the ratio of the number of detection events to the number of incident photons and includes the transmission and alignment of the microlens array (50–80 %), avalanche probability (60% for an overbias level of 4 V), and the quantum efficiency of the APD (about 95%) [12]. As the incident photon number approaches the number of detector elements, the chance of a photon hitting a pixel that has already fired increases. This blocking effect causes the PDE to decrease with increasing photon flux.

The PDE can be computed using a Monte Carlo technique. In our simulations we assume that the laser pulse width is much shorter than the detector reset time. The input parameters to our Monte Carlo simulation are the average number of photons in the pulse, the number of pixels in the array, the single-element PDE, and the 2D-intensity beam profile on the array. The number of photons per pulse was assumed to follow Poissonian statistics. The net PDE is com-

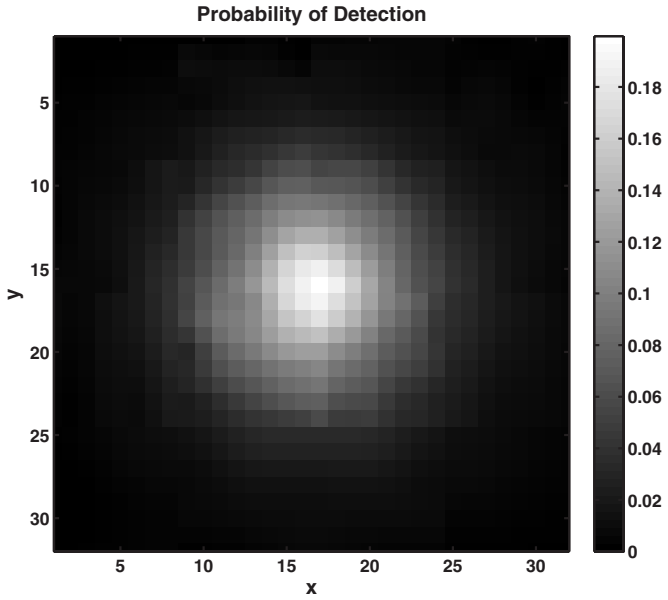

FIG. 3. Probability of detection for the pulsed laser source at an average power of −94.65 dBm.

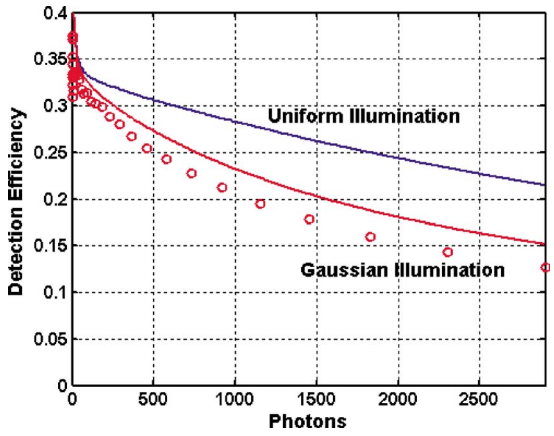

FIG. 4. (Color online) Detection efficiency vs the number of incident photons. The circles are measurements and the solid lines are Monte Carlo simulations.

puted as a function of the average number of incident photons using the following algorithm.

(1) For each pixel, assign an average number of incident photons per pulse that is equal to the product of the total photons per optical pulse and the value of a probability density function describing the 2D beam intensity profile at that pixel. This number is then multiplied by the PDE to obtain an average number of detected photons per pulse at that pixel. The fact each pixel cannot count more than one photon at a time is treated in step (3) below.

(2) For each pixel, assign an average number of dark counts. There are roughly 0.74 dark counts per 4.5 ns period over the 1024 detectors. The 4.5 ns period corresponds to the integration window used in our experiments.

(3) Randomly mark each pixel as fired or not fired. The probability that a pixel is marked fired is equal to 1 −exp[−average detected photons−average dark counts], using the averages calculated per pulse for that pixel in steps (1) and (2). Thus the probability a pixel fires is described by a Poisson distribution.

(4) After all pixels have been marked, sum the number of "fired pixels" to determine the number of detection events for this given pulse.

(5) Repeat steps (1) through (4) 10 000 times (average over 10 000 pulses) and keep track of the number of detection events. The mean of the number of detection events with the optical pulse (minus the mean number of detection events with no optical pulse) divided by the number of incident photons is the net PDE.

The net PDE is plotted as a function of incident photon number in Fig. 4. The solid lines represent the Monte Carlo simulation results for a 33% single-element PDE, 1024 total pixels, and a 2D beam intensity profile given by Fig. 3. There were 45 bad pixels, mostly along the perimeter of the detector that had a 0% PDE. The data, shown with circles in Fig. 4, shows that the PDE decreases from 33% with 1 incident photon to 21% with 1024 incident photons. This decrease in detection efficiency with increasing photon number is due to the finite number of detectors and the increasing fraction of inactive pixels with increasing incident photons. The performance can be improved with uniform illumination of the detector array to a PDE of 28% with 1024 photons. Refractive beam shapers that transform a Gaussian beam profile to a flat top beam profile are commercially available optical components. The simulated curve in Fig. 4 for Gaussian illumination matches well to the measured results.

The measured PDE is plotted with circles in Fig. 4 and is computed by dividing the number of detection events integrated in a 4.5 ns interval around the pulse arrival time by the number of incident photons. The number of incident photons was computed by subtracting the attenuator value from the measured nonattenuated power level. The integration range was set to 4.5 ns to ensure that the entire pulse was captured. The data, shown with circles in Fig. 4, show that the PDE decreases from 33% with 1 incident photon to 21% with 1024 incident photons. The unsaturated PDE is measured at 33% but values as high as 50% have been measured in some of our other detectors [11]. Figure 4 shows that the measured results are accurately predicted by the Monte Carlo simulations. We also note that the PDE is still rather large, 13% (21% for uniform illumination), at 3000 incident photons.

The fidelity, or similarly, the ability to identify n from $n+1$ photons, is an important metric for quantum optics applications. We define fidelity as the probability of measuring n detection events when n photons are incident on the detector. Ignoring dark counts, which will not be treated here, fidelity is degraded by two effects in the Geiger-mode APD array approach: Detection efficiency and detector saturation. The fidelity, F, is approximately equal to the product $F_{\text{det}}F_{\text{sat}}$, where F_{det} is the fidelity with just detection efficiency degradation and F_{sat} is the fidelity with just detector saturation degradation. The fidelity of a detector with a detection efficiency of PDE is equal to $F_{\text{det}}=(\text{PDE})^n$. For our detector, PDE=0.33, so, for example, $F_{\text{det}}=0.004$ for $n=5$ incident photons. To derive F_{sat}, we assume that each pixel is equally likely to be hit by a photon (ignoring beam shape). The probability that n photons hit n different pixels on an array of N detectors is

$$F_{\text{sat}} = \frac{N}{N}\frac{N-1}{N}\frac{N-2}{N}\frac{N-3}{N}\cdots\frac{N-(n-1)}{N} = \frac{N!}{N^n(N-n)!}. \tag{1}$$

Therefore, the saturation factor of an $N=1024$-element detector in discriminating $n=5$ photons is $F_{\text{sat}}=0.99$. This shows that F_{sat} is excellent when $N \leqslant n$. The total fidelity for $n=5$ is equal to $F=F_{\text{det}}F_{\text{sat}}\sim 0.004$, and hence the fidelity is dominated by the detection efficiency of the detector, that is, it is the PDE and not the blocking that is limiting the fidelity. To increase the usefulness of the presented detector for quantum optics measurements, the detection efficiency must be improved.

The contributions to the fidelity are actually different for detectors that use pulse-height discrimination to achieve photon-number resolution as compared to our array approach. The saturation term above, F_{sat}, should be replaced by a term representing all errors due to noise in the pulse-height measurement including noise and saturation effects.

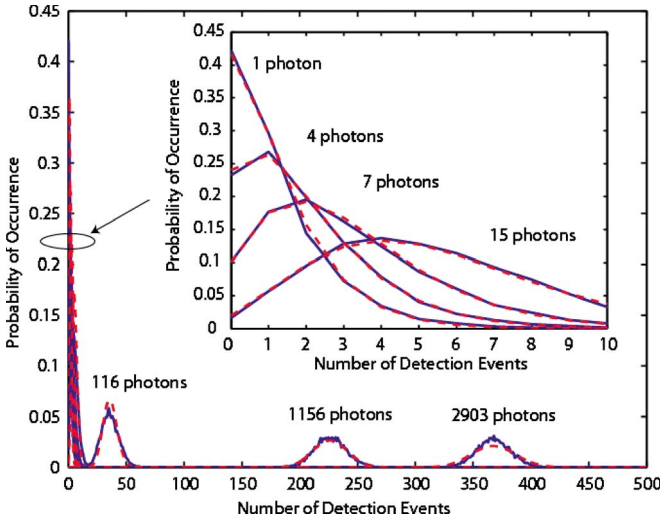

FIG. 5. (Color online) The probability of occurrence as a function of the number of detection events for different incident power levels. Solid lines are experimentally measured values and dashed lines are theoretical curves corresponding to Poisson statistics for 116, 1156, and 2903 photons. The data are fit to a negative binomial distribution [13] with $(M,\bar{K})$ equal to (2.0,1.1), (2.6,1.9), (4.0,3.1), and (6.0,5.5) for 1, 4, 7, and 15 photons, respectively. The parameter M represents the number of degrees of freedom of the intensity within the measurement interval and $\bar{K}$ is the average number of photoelectrons.

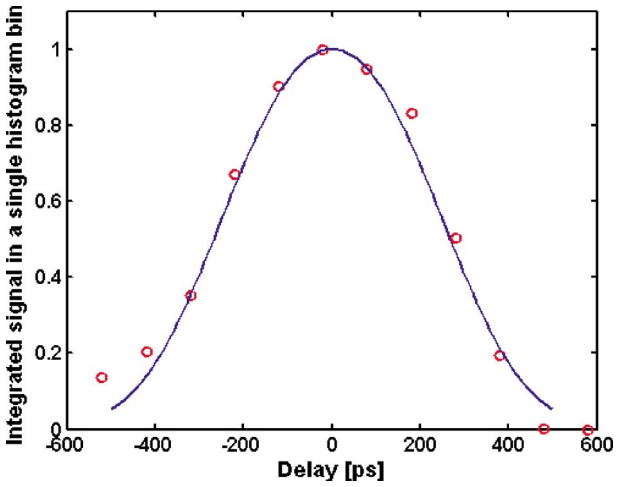

FIG. 6. (Color online) Integrated signal in a single histogram time bin as a function of delay. The data are shown with circles and the solid line is a theoretical fit corresponding to an rms timing jitter of 133 ps, pulse width of 70 ps, and time bin of 500 ps.

Our array approach uses single-photon counting elements that only differentiate between zero and one photons, so any pulse-height-measurement errors are included in the detection efficiency and hence this term is not necessary in the expression for fidelity discussed previously. The degradation in fidelity due to pulse-height-measurement errors are typically large compared to the saturation effect in our array. Similarly, it is these errors that limit pulse-height-measuring, photon-number-resolving detectors to only a few bits of resolution, while we demonstrate 10 bits with the array approach.

The probability of obtaining a given number of detection events for various incident photon flux levels is plotted in Fig. 5. The average input photon number per pulse from the PicoQuant laser was set with the variable optical attenuator to 1, 4, 7, 15, 116, 1156, and 2903 photons. For each power setting, the number of detection events per pulse was recorded. The probability density function for a given power level in Fig. 5 was computed by histogramming the number of detection events taken over 10 000 pulses and dividing the histogram by 10 000. The solid lines in Fig. 5 are the measured results and the dashed lines are Poissonian probability density functions with the same mean. At low photon fluxes (1 to 15 photons), inset of Fig. 5, the detected photon number distribution are fit with negative binomial distributions to account for laser intensity noise and background room light. At high photon fluxes (116 to 2903 photons), both the measured and Poissonian distributions approach a Gaussian shape.

The timing jitter of each individual APD is typically smaller than the 0.5 ns counter resolution. Since readout ICs with higher clock rates are being planned, it is important to characterize the actual timing jitter of the APD. The timing jitter of each pixel can be obtained from a "knife-edge" measurement—except that this knife edge occurs in time rather than space. The relative laser pulse-to-APD trigger delay can be tuned with picosecond resolution with the dual-channel pulse generator. The APD timing jitter is obtained by tuning the laser pulse-to-APD trigger delay in 100 ps steps, histogramming the photon arrival times from one APD in the array, and measuring the energy in one of the 0.5 ns time bins versus delay. The time bin is assumed to have a square shape. As the delay is swept, the optical pulse is swept through the selected time bin and the integrated signal increases as the optical pulse enters the selected time bin and then decreases as the optical pulse passes the selected time bin. The integrated signal in a single histogram time bin is plotted as a function of delay in Fig. 6 and the width of the plot is related to the timing jitter, optical pulse width, time bin width, and trigger jitter. Assuming that the trigger jitter is negligible and that the timing jitter and pulse shape are Gaussian, we can fit the data (circles) in Fig. 6 with the theoretically expected shape (solid line). The solid line in Fig. 6 corresponds to a Gaussian with a standard deviation of 150 ps convolved with a 0.5 ns time bin. The rms timing jitter is 133 ps assuming an optical pulse width of 70 ps. The slight deviation of the theoretical curve from the data is due to the fact that (1) the timing jitter and optical pulse shape are not perfect Gaussians and (2) that the time bin is not perfectly square shaped.

IV. SUMMARY

We have demonstrated a 10-bit resolution photon-number-resolving detector sensitive 1.06 μm light with 33% detection efficiency, a dark count rate of 160 000 counts/s per

pixel, and 133 ps timing jitter. This is the highest number of bits of resolution reported to date and the increased dynamic range enables new applications in coherent laser radar and 3D laser radar. By using an array with digital electronics behind every pixel, the measured count rate is not affected by multiplication noise in the detector or electrical noise from analog readout. The only sources of noise are the dark counts and the shot noise. Using part of the APD array allows one to trade off resolution for reduced dark counts.

ACKNOWLEDGMENTS

The authors thank Jan Kleyna and Jane Luu for the helpful simulation code and clever insight.

[1] M. A. Albota, B. F. Aull, D. G. Fouche, R. M. Heinrichs, D. G. Kocher, R. M. Marino, J. G. Mooney, N. R. Newbury, M. E. O'Brien, B. E. Player, B. C. Willard, and J. J. Zayhowski, Lincoln Lab. J. **13**, 351 (2002).

[2] J. X. Luu and L. A. Jiang, Appl. Opt. **45**, 3798 (2006).

[3] E. Knill, R. Laflamme, and G. J. Milburn, Nature (London) **409**, 46 (2001).

[4] R. H. Hadfield, M. J. Stevens, S. S. Gruber, A. J. Miller, R. E. Schwall, R. P. Mirin, and S. W. Nam, Opt. Express **13**, 10846 (2005).

[5] E. Waks, K. Inoue, W. D. Oliver, E. Diamanti, and Y. Yamamoto, IEEE J. Sel. Top. Quantum Electron. **9**, 1502 (2003); D. Rosenberg, A. E. Lita, A. J. Miller, and S. W. Nam, Phys. Rev. A **71**, 061803 (2005).

[6] M. J. Fitch, B. C. Jacobs, T. B. Pittman, and J. D. Franson, Phys. Rev. A **68**, 043814 (2003); O. Haderka, M. Humar, and J. Perina, Jr., Eur. Phys. J. D **28**, 149 (2004).

[7] M. Akiba, M. Fujiwara, and M. Sasaki, Opt. Lett. **30**, 123 (2005).

[8] S. Song, C. M. Caves, and B. Yurke, Phys. Rev. A **41**, 5261 (1990).

[9] E. A. Dauler, B. S. Robinson, A. J. Kerman, J. K. W. Yang, K. M. Rosfjord, V. Anant, B. Voronov, G. Gol'tsman, and K. K. Berggren, IEEE Trans. Appl. Supercond. (to be published).

[10] S. Verghese, D. M. Cohen, E. A. Dauler, J. P. Donnelly, E. K. Duerr, S. H. Groves, P. I. Hopman, K. E. Jensen, Z.-L. Liau, L. J. Mahoney, K. A. McIntosh, D. C. Oakley, and G. M. Smith, *IEEE 2005 Digest of the LEOS Summer Topical Meetings* (IEEE, Piscataway, NJ, 2005), p. 15; K. E. Jensen, P. I. Hopman, E. K. Duerr, E. A. Dauler, J. P. Donnelly, S. H. Groves, L. J. Mahoney, K. A. McIntosh, K. M. Molvar, A. Napoleone, D. C. Oakley, S. Verghese, C. J. Vineis, and R. D. Younger, Appl. Phys. Lett. **88**, 133503 (2006).

[11] E. A. Dauler, P. I. Hopman, K. A. McIntosh, J. P. Donnelly, E. K. Duerr, R. J. Magliocco, L. J. Mahoney, K. M. Molvar, A. Napoleone, D. C. Oakley, and F. J. O'Donnell, Appl. Phys. Lett. **89**, 111102 (2006).

[12] J. P. Donnelly, K. A. McIntosh, D. C. Oakley, A. Napoleone, S. H. Groves, S. Vernon, L. J. Mahoney, K. Molvar, J. Mahan, J. C. Aversa, E. K. Duerr, Z. L. Liau, B. F. Aull, and D. C. Shaver, *Laser Radar Technology and Applications X*, Proc. SPIE (SPIE, Bellingham, WA, 2005), p. 281.

[13] J. W. Goodman, *Statistical Optics* (Wiley, New York, 1985), p. 476.